Impact of RF Processing and Switching Errors in Lens–Based Massive MIMO Systems (Invited Paper)

Impact of RF Processing and Switching Errors in Lens–Based Massive MIMO Systems

Harsh Tataria*, Michail Matthaiou*, Peter J. Smith†, George C. Alexandropoulos‡, and Vincent F. Fusco*
*Institute of Electronics, Communications and Information Technology (ECIT), Queen's University Belfast, Belfast, U.K.
†School of Mathematics and Statistics, Victoria University of Wellington, Wellington, New Zealand
‡Mathematical and Algorithmic Sciences Lab, Paris Research Center, Huawei Technologies France SASU, France
e–mail:{h.tataria, m.matthaiou, v.fusco}@qub.ac.uk, peter.smith@vuw.ac.nz, and george.alexandropoulos@huawei.com

***Abstract*—Lens–based massive multiple–input multiple–output (MIMO) systems have considerable potential to reduce signal processing cost at millimeter–wave frequencies. As a result, they are able to lower the effective channel dimension via beam selection, realized with a network of radio–frequency (RF) switches. However, lens arrays suffer from the inherent quantization of the beamspace, as well as errors due to imperfections in the lens construction itself. Unlike prior works, we model the above effects in the context of a Rotman lens–enabled massive MIMO system. Assuming line–of–sight propagation, we derive analytical approximations of the expected (average) signal–to–interference–plus–noise–ratio (SINR) of a terminal and ergodic sum spectral efficiency of the system. Our analysis caters for spillover losses in the Rotman lens and imperfections in the RF switching matrix, caused by impedance mismatches, as well as poor port isolation. The presented numerical results show large degradation in the expected SINR and ergodic spectral efficiency when considering the above imperfections, yielding more accurate performance assessment of lens–based massive MIMO systems.**

I. Introduction

It is now clear that millimeter–wave (mmWave) frequencies will play a significant role in future mobile broadband access [1]. However, operation at such high frequencies has led to new challenges which must be overcome before their large–scale deployment. Relative to centimeter–wave frequencies, propagation at mmWave is different due to the high path loss and inefficiency of diffraction. The dominant mmWave propagation mechanisms are unobstructed line–of–sight (LOS) and specular reflections, causing the channel to be sparse and directional [2]. Hence, to effectively transmit a signal over moderate distances, mmWave systems need large array gains, requiring the use of massive arrays at the base station (BS). Nevertheless, if contemporary multiuser multiple–input multiple–output (MIMO) techniques are employed with such large arrays, the corresponding signal processing (SP) cost and hardware complexity increases exponentially, since each element requires a dedicated radio–frequency (RF) chain.

Extensive research efforts have been made to reduce the SP complexity with techniques such as hybrid (RF–baseband) processing (see e.g., [3–5]). Advanced antenna arrays containing RF lenses have also been studied to complement hybrid SP [2, 6–9]. Fundamentally, RF lenses are phase shifting devices, which convert a divergent waveform from a point source to a plane wave. Moreover, RF lenses enhance the directive gain of the array, providing *direction–specific* spatial focusing of electromagnetic radiation. This is of particular importance in sparse mmWave channels, as the effective signal dimension can be reduced in the RF domain via a bank of RF switches which perform beam selection. A common topology in the literature is referred to as the *Rotman lens*, which utilizes a uniform linear array (ULA) for signal transmission/reception [7, 9]. In this light, discrete lens arrays were considered for massive MIMO systems in [2]. The literature also reports the use of flat RF lenses, where unlike the Rotman structure, the antenna elements are non–uniformly spaced on the focal arc of the lens (see, e.g., [8] and references therein).

Having said this, almost all of the above work assumes that the lens is a *perfect* reciprocal device. This is highly unlikely due to the inherent nonlinearities that are inevitable from the lens construction. Such nonlinearities often lead to *aberration* in the spatial focusing of signals, causing *spillover losses* – as RF power desired for a particular beam port also *leaks* into neighboring beam ports. Furthermore, the above studies also assume that both the RF and baseband SP functionalities are ideal. To this end, *perfect* RF switching is routinely assumed *irrespective* of the size of the switch matrix. In reality, this is also not the case, since the standard diode/transistor–driven single–pole multiple–throw switches do not have perfect *absorption* and *isolation characteristics*. As a result, they are prone to *impedance mismatches*, and *poor port–to–port isolation*, causing return loss of RF power to multiple beam ports with high voltage standing wave ratios. This is typically observed in moderately large RF switches operating at mmWave frequencies [10]. To the best of our knowledge, the *aggregate* impact of the above imperfections on multiuser massive MIMO performance is missing from the literature. In this paper, we close this gap by mathematically modeling the aforementioned impairments and analyzing the system performance in the context of a Rotman lens. Assuming LOS propagation and uplink maximum–ratio combining (MRC), we develop tight analytical approximations of the expected (average) signal–to–interference–plus–noise–ratio (SINR) of a given terminal, and ergodic sum spectral efficiency of the system. Analyses of such type are extremely challenging due to the *joint* operation of RF and baseband SP. The developed expressions are general and remain accurate across a wide range of transmit and receive dimensions, as well as operating signal–to–noise–ratios (SNRs). Our numerical results show

The work of H. Tataria and M. Matthaiou was supported by the EPSRC, UK, under grant EP/P000673/1. The work of V. F. Fusco was supported by the EPSRC, UK, under grant EP/EN02039/1.

that the expected SINR and ergodic sum spectral efficiency decrease significantly when we consider the aggregate impact of a non–ideal lens with imperfect RF switching, yielding more accurate performance assessment of lens–based architectures.

Notation. Boldface upper and lower case symbols are used to denote matrices and vectors. The $M \times M$ identity matrix is denoted by $\mathbf{I}_M$. The transpose, conjugate, and Hermitian transpose operations are denoted by $(\cdot)^T$, $(\cdot)^*$, and $(\cdot)^H$, respectively. We use $\mathbf{m} \sim \mathcal{CN}(0, \sigma^2)$ to denote independent and identically distributed (i.i.d.) random entries in the vector $\mathbf{m}$ having complex Gaussian distribution with zero–mean and variance σ^2. Furthermore, $m \sim \mathcal{U}[a, b]$ is used to denote an i.i.d. uniform random variable m, taking on values from a to b. Finally, the statistical expectation, matrix trace, and scalar norm operations are denoted by $\mathbb{E}[\cdot]$, $\mathrm{Tr}[\cdot]$ and $|\cdot|$, respectively.

II. System Model

The uplink of a single–cell system is considered, where the BS contains an N element Rotman lens array receiving data from L single–antenna terminals ($L \ll N$). LOS propagation is assumed between the terminals and the BS. The terminals are uniformly distributed in a circular area with radius R_{c}, and the BS is located at the origin of this circle.

Remark 1. *With LOS propagation, acquisition of a complete channel response at the BS is not required, since only the uplink direction–of–arrivals (DOAs) need to be estimated. With lens antenna arrays, these are recovered with sufficient accuracy from the unique spatial mapping between each antenna and beam port. Moreover, as the DOAs vary slowly relative to small–scale fading, they can be estimated over multiple channel coherence intervals exploiting reciprocity.*

A. Perfect Rotman Lens and RF Switching

The Rotman array decouples the L multiplexed streams with RF and baseband SP. Specifically, the N elements form N fixed analog beam directions, $\phi_1, \phi_2, \ldots, \phi_N$. The L terminals are then selected to occupy L *separate* subports via the switching network. To begin with, we assume that both the lens and the RF switch matrix have ideal characteristics. The dimension–reduced signal after beam selection is down–converted via L RF transceivers and digitized before MRC. The $L \times 1$ received signal after beam selection is given by

$$\mathbf{y} = \rho_{\mathrm{t}}^{\frac{1}{2}} \mathbf{S}_{\mathrm{RF}} \mathbf{F}_{\mathrm{RF}} \mathbf{H} \mathbf{x} + \mathbf{n} = \rho_{\mathrm{t}}^{\frac{1}{2}} \mathbf{G} \mathbf{x} + \mathbf{n}, \tag{1}$$

where $\mathbf{G} = [\mathbf{g}_1\ \mathbf{g}_2, \ldots, \mathbf{g}_L]$ is an $L \times L$ matrix such that the $L \times 1$ vector $\mathbf{g}_\ell = \mathbf{S}_{\mathrm{RF}} \mathbf{F}_{\mathrm{RF}} \mathbf{h}_\ell$, $\forall \ell = 1, 2, \ldots, L$. Moreover, the $N \times 1$ LOS vector from terminal ℓ to the BS is given by

$$\mathbf{h}_\ell = \alpha_\ell^{\frac{1}{2}} N^{\frac{1}{2}} \mathbf{a}(\varphi_\ell). \tag{2}$$

In (2), $\alpha_\ell = d_\ell^{-\eta}$ denotes the link gain composed of distance–dependent path loss at distance d_ℓ from the BS array to terminal ℓ with attenuation exponent η. The complex array steering vector for a DOA φ_ℓ, from terminal ℓ is given by

$$\mathbf{a}(\varphi_\ell) = N^{-\frac{1}{2}} \left[1\ e^{jk_0 \Delta \sin(\varphi_\ell)}, \ldots, e^{jk_0 (N-1) \Delta \sin(\varphi_\ell)}\right]^T. \tag{3}$$

The constant $k_0 = 2\pi/\lambda$ denotes the wavenumber with wavelength λ at the operational carrier frequency, f_{c}, while Δ denotes the inter–element spacing between two adjacent elements in the ULA. Furthermore, $\rho_{\mathrm{t}}^{1/2}\mathbf{x}$ is the $L \times 1$ vector of uplink payload data, where the average transmit power of each terminal is ρ_{t}, with $\mathbb{E}[|x_\ell|^2] = 1, \forall \ell = 1, 2, \ldots, L$. The net functionality of an ideal Rotman lens with perfect focusing capability is described by the $N \times N$ matrix, $\mathbf{F}_{\mathrm{RF}}$, such that

$$\mathbf{F}_{\mathrm{RF}} = \left[\mathbf{a}^H(\phi_1)\ \mathbf{a}^H(\phi_2), \ldots, \mathbf{a}^H(\phi_N)\right]^T. \tag{4}$$

Note that each vector in (4) follows the same structure as (3). A subset of directions, $\phi_1, \phi_2, \ldots, \phi_L$ (corresponding to L terminals), are then selected via an $L \times N$ RF switching network, $\mathbf{S}_{\mathrm{RF}}$. With perfect switching, $\mathbf{S}_{\mathrm{RF}}$ is a binary matrix and each row of it contains only one non–zero entry corresponding to the selected beam index. The $L \times 1$ vector of additive Gaussian noise is denoted by $\mathbf{n}$, where each entry of $\mathbf{n} \sim \mathcal{CN}(0, 1)$.

B. Imperfect Rotman Lens and RF Switching

To facilitate the later analysis, we relabel the selected beam directions such that $\mathbf{S}_{\mathrm{RF}}$ contains an $L \times L$ identity matrix, concatenated with an $L \times (N - L)$ matrix of zeros. We also assume that $\mathbf{F}_{\mathrm{RF}}$ is ordered by the selected beams. *As the switches are not fully absorptive, each input port of the switch is likely to reflect RF energy back towards the lens beam ports. Moreover, due to poor port isolation, energy is also likely to couple to neighboring ports in the switch. Since the reflected voltages are complex quantities, the imperfect switching matrix is modeled to have complex entries, with the off–diagonals of the matrix being non–zero and typically 20 dB lower in magnitude relative to the selected port [10].* We denote the imperfect switching matrix as $\widetilde{\mathbf{S}}_{\mathrm{RF}} = \mathbf{S}_{\mathrm{RF}} + \mathbf{\Xi}$, where the (r, s)–th entry of $\mathbf{\Xi}$, denoted by $[\mathbf{\Xi}]_{r,s} = e_{r,s} \sim \mathcal{CN}(0, \sigma_{\mathrm{E}}^2)$. Here, σ_{E} controls the level of return loss. *Similarly, as an imperfect Rotman lens loses the ability to focus a particular DOA to a specific beam port, spillover losses are caused to neighboring ports.* The (r, s)–th element of the imperfect Rotman lens matrix, $\widetilde{\mathbf{F}}_{\mathrm{RF}}$, is denoted by

$$[\widetilde{\mathbf{F}}_{\mathrm{RF}}]_{r,s} = \tilde{f}_{r,s} = \left(\widetilde{\mathbf{a}}_r^H\right)_s = \underbrace{N^{-\frac{1}{2}} e^{-jk_0(s-1)\Delta \sin(\phi_r)}}_{\text{Perfect component, } (\mathbf{a}_r^H)_s = f_{r,s}} e^{j\delta_{r,s}}, \tag{5}$$

where $\delta_{r,s} \sim \mathcal{CN}(0, \epsilon^2)$, where ϵ controls the level of spillover loss. For ease of notation, $\widetilde{\mathbf{a}}_r$ is the shorthand for $\widetilde{\mathbf{a}}(\phi_r)$.

Remark 2. *It is interesting to observe that the relationship between $f_{r,s}$ and $\tilde{f}_{r,s}$ satisfies the subsequent conditions:*

- *Both $f_{r,s}$ and $\tilde{f}_{r,s}$ have the same power. That is, $\mathbb{E}[|f_{r,s}|^2] = \mathbb{E}[|\tilde{f}_{r,s}|^2] = 1/N$.*
- *The correlation between $f_{r,s}$ and $\tilde{f}_{r,s}$ is proportional to $e^{-\epsilon^2/2}$, i.e., $\mathbb{E}[f_{r,s}\tilde{f}_{r,s}^*] = \mathbb{E}[f_{r,s}f_{r,s}^* e^{-j\delta_{r,s}}] = 1/N\,(e^{-\epsilon^2/2})$.*
- *For small ϵ values, we have $\tilde{f}_{r,s} \approx f_{r,s}(1 + j\delta_{r,s})$. Thus, conditioned on $f_{r,s}$, $\tilde{f}_{r,s}$ is also Gaussian distributed.*

Satisfying the above conditions, we propose an alternative model for $\tilde{f}_{r,s}$ which is much simpler to analyze than the originally proposed Gaussian error model for the considered performance metrics. We let $\varsigma = e^{-\epsilon^2/2}$ and express $\tilde{f}_{r,s}$ as:

$$\tilde{f}_{r,s} = \varsigma f_{r,s} + \left(\frac{1 - \varsigma^2}{N}\right)^{\frac{1}{2}} \tilde{e}_{r,s} = \varsigma f_{r,s} + \kappa \tilde{e}_{r,s}, \tag{6}$$

where $\tilde{e}_{r,s} \sim \mathcal{CN}(0,1)$. Assuming $\kappa \ll \varsigma$, for small values of ϵ, this simple model yields

$$[\widetilde{\mathbf{F}}_{\text{RF}}]_{r,s} = \varsigma N^{-\frac{1}{2}} e^{-jk_0(s-1)\Delta \sin(\phi_r)} + \kappa \tilde{e}_{r,s}. \quad (7)$$

Except for the above differences in the Rotman lens matrix and the RF switch matrix, the remainder of the model remains as in Sec. II-A. For notational consistency, we define the erroneous version of $\mathbf{g}_\ell$ as $\widetilde{\mathbf{g}}_\ell$, $\forall \ell = 1, 2, \ldots, L$.

C. MRC SINR and Ergodic Sum Spectral Efficiency

From (1), with MRC at the BS and noise variance of σ^2, the SINR of terminal ℓ with an imperfect lens and RF switching matrix is given by

$$\text{SINR}_\ell = \frac{\rho_{\text{t}} \left|\widetilde{\mathbf{g}}_\ell^H \widetilde{\mathbf{g}}_\ell\right|^2}{\sigma^2 \widetilde{\mathbf{g}}_\ell^H \widetilde{\mathbf{g}}_\ell + \rho_{\text{t}} \sum\limits_{\substack{i=1 \\ i\neq\ell}}^{L} \left|\widetilde{\mathbf{g}}_\ell^H \widetilde{\mathbf{g}}_i\right|^2}. \quad (8)$$

For a given instance of $\widetilde{\mathbf{g}}_\ell$ and $\widetilde{\mathbf{g}}_i$, SINR_ℓ can be translated into an instantaneous spectral efficiency (in bit/sec/Hz) for terminal ℓ via $\text{R}_\ell = \log_2(1+\text{SINR}_\ell)$. This can be used to compute the ergodic sum spectral efficiency of the system via

$$\text{R}_{\text{sum}} = \mathbb{E}\left[\sum_{\ell=1}^{L} \text{R}_\ell\right]. \quad (9)$$

III. Expected SINR and Ergodic Sum Spectral Efficiency Approximations

Remark 3. *Before presenting the main analytical contributions of the paper, we list some preliminary mathematical results that are referred to throughout the section. Using the classical properties of zero–mean complex Gaussian random variables:*

- *We first note that $\mathbb{E}[\boldsymbol{\Xi}] = \mathbf{0}$.*
- *The correlation matrix of $\boldsymbol{\Xi}$, is obtained as*

$$\mathbb{E}[\boldsymbol{\Xi}^H \boldsymbol{\Xi}] = (\sigma_{\text{E}}^2 L)\mathbf{I}_L. \quad (10)$$

- *For any Hermitian matrix $\boldsymbol{\Pi}$,*

$$\mathbb{E}[\boldsymbol{\Xi}\boldsymbol{\Pi}\boldsymbol{\Xi}^H] = \sigma_{\text{E}}^2 \,\text{Tr}[\boldsymbol{\Pi}]\,\mathbf{I}_L. \quad (11)$$

- *From the previous result, we note that*

$$\mathbb{E}[\boldsymbol{\Xi}^H\boldsymbol{\Xi}\boldsymbol{\Pi}\boldsymbol{\Xi}^H\boldsymbol{\Xi}] = \left(\sigma_{\text{E}}^4 L\right)\boldsymbol{\Pi} + \left(\sigma_{\text{E}}^4 L\right)\mathbf{I}_L \text{Tr}[\boldsymbol{\Pi}]. \quad (12)$$

- *For a given instance of $\mathbf{h}_\ell$, $\mathbf{h}_\ell^H \mathbf{h}_\ell = \alpha_\ell N$.*

Now, from (8), the expected SINR for terminal ℓ can be obtained by computing $\mathbb{E}[\text{SINR}_\ell]$. As the exact evaluation of $\mathbb{E}[\text{SINR}_\ell]$ is extremely challenging, we employ the common first–order Laplace approximation, which yields [11]

$$\mathbb{E}\left[\text{SINR}_\ell\right] \approx \frac{\rho_{\text{t}} \mathbb{E}\left[\left|\widetilde{\mathbf{g}}_\ell^H \widetilde{\mathbf{g}}_\ell\right|^2\right]}{\sigma^2 \mathbb{E}\left[\widetilde{\mathbf{g}}_\ell^H \widetilde{\mathbf{g}}_\ell\right] + \rho_{\text{t}} \sum\limits_{\substack{i=1 \\ i\neq\ell}}^{L} \mathbb{E}\left[\left|\widetilde{\mathbf{g}}_\ell^H \widetilde{\mathbf{g}}_i\right|^2\right]}. \quad (13)$$

Taking the expectation over the errors in the switching matrix, the numerator of (13) can be written as

$$\rho_{\text{t}} \mathbb{E}\left[\left|\widetilde{\mathbf{g}}_\ell^H \widetilde{\mathbf{g}}_\ell\right|^2\right] = \rho_{\text{t}}\, (\alpha_\ell N)^2 \left[p_2 + 2\,(L+1)\, p_1\, \sigma_{\text{E}}^2 + L\,(L+1)\,\sigma_{\text{E}}^2\right], \quad (14)$$

where the constants

$$p_1 = \mathbb{E}\left[\mathbf{a}^H(\varphi_\ell)\, \boldsymbol{\Delta}_1^H \boldsymbol{\Delta}_1\, \mathbf{a}\,(\varphi_\ell)\right], \quad (15)$$

and

$$p_2 = \mathbb{E}\left[\left(\mathbf{a}^H(\varphi_\ell)\, \boldsymbol{\Delta}_1^H \boldsymbol{\Delta}_1\, \mathbf{a}\,(\varphi_\ell)\right)^2\right]. \quad (16)$$

The matrix $\boldsymbol{\Delta}_1$ is defined by $\boldsymbol{\Delta}_1 = \mathbf{S}_{\text{RF}} \widetilde{\mathbf{F}}_{\text{RF}}$. Since the expectations in p_1 and p_2 are over the imperfections in the RF switching matrix, $\boldsymbol{\Delta}_1$ now only relies on the imperfect Rotman matrix, $\mathbf{F}_{\text{RF}}$. We note that (14) only requires expansion of $|\widetilde{\mathbf{g}}_\ell^H \widetilde{\mathbf{g}}_\ell|^2$, followed by application of the preliminary results and algebraic simplifications. The same method also allows us to write the expected noise power as

$$\sigma^2 \mathbb{E}\left[\widetilde{\mathbf{g}}_\ell^H \widetilde{\mathbf{g}}_\ell\right] = \alpha_\ell \sigma^2 N \left(p_1 + \sigma_{\text{E}}^2 L\right), \quad (17)$$

and the expected interference power as

$$\rho_{\text{t}} \sum_{\substack{i=1 \\ i\neq\ell}}^{L} \mathbb{E}\left[\left|\widetilde{\mathbf{g}}_\ell^H \widetilde{\mathbf{g}}_i\right|^2\right] = \rho_{\text{t}} \sum_{\substack{i=1 \\ i\neq\ell}}^{L} \alpha_\ell \alpha_i N^2 \left[p_4 + \sigma_{\text{E}}^2 L\,(p_5 + p_5^*) + \sigma_{\text{E}}^2\,(p_1 + \tilde{p}_1) + \sigma_{\text{E}}^4 L\, p_3 + \sigma_{\text{E}}^4 L\right]. \quad (18)$$

More specifically, the constants

$$p_4 = \mathbb{E}\left[\left|\mathbf{a}^H(\varphi_\ell)\, \boldsymbol{\Delta}_1^H \boldsymbol{\Delta}_1\, \mathbf{a}\,(\varphi_i)\right|^2\right], \quad (19)$$

$$\tilde{p}_1 = \mathbb{E}\left[\mathbf{a}^H(\varphi_i)\, \boldsymbol{\Delta}_1^H \boldsymbol{\Delta}_1\, \mathbf{a}\,(\varphi_i)\right], \quad (20)$$

$$p_3 = \mathbb{E}\left[\left|\mathbf{a}^H(\varphi_\ell)\, \mathbf{a}(\varphi_i)\right|^2\right], \quad (21)$$

and

$$p_5 = \mathbb{E}\left[\mathbf{a}^H(\varphi_\ell)\, \mathbf{a}\,(\varphi_i)\, \mathbf{a}^H(\varphi_i)\, \boldsymbol{\Delta}_1^H \boldsymbol{\Delta}_1\, \mathbf{a}\,(\varphi_\ell)\right]. \quad (22)$$

Remark 4. *It is interesting to observe that both the signal and interference power constants are expressed in terms of quadratic forms of the desired and interfering DOAs, φ_ℓ and φ_i. For a fixed $\boldsymbol{\Delta}_1^H \boldsymbol{\Delta}_1$, p_4, $\tilde{p}_1$, p_3 and p_5 yield a larger value when φ_ℓ and φ_i are aligned. This amplifies the interference power leading to a lower expected SINR. Now, since the terminals are i.i.d., we can simplify the expected SINR for terminal ℓ by noting that $p_1 = \tilde{p}_1$. This allows us to write* (23) *on top of the following page. Using the background results, expanding the quadratic forms in p_1, taking the expectation over the LOS angles as well as the selected bins, and dropping the higher–order terms in σ_{E}^4 (since $\sigma_{\text{E}}^4 \ll \sigma_{\text{E}}^2$) yields the result in* (24) *on top of the following page. Note that m_1, m_2, m_4, and m_5 are the expected values of p_1, p_2, p_4, and p_5 over $\tilde{e}_{r,s}$. In the analysis which follows, we solve for m_1, m_2, m_4 and m_5. We show a method to compute m_1 and quote the results for m_2, m_4 and m_5 since they follow from the same process.*

In particular,

$$m_1 = \varsigma^2 \mathbb{E}\left[\mathbf{a}^H(\varphi_\ell) \sum_{i=1}^{L} \mathbf{a}\,(\phi_i)\, \mathbf{a}^H(\phi_i)\, \mathbf{a}\,(\varphi_\ell)\right] + \mathcal{O}\left(\kappa^2\right) \quad (25)$$

$$\approx \varsigma^2 \mathbb{E}\left[\mathbf{a}^H(\varphi_1)\, \mathbf{a}\,(\phi_1)\, \mathbf{a}^H\,(\phi_1)\, \mathbf{a}\,(\varphi_1)\right] + \varsigma^2 \mathbb{E}\left[\frac{(L-1)}{(N-1)} \sum_{s=2}^{N} \mathbf{a}^H(\varphi_1)\, \mathbf{a}\,(\phi_s)\, \mathbf{a}^H(\phi_s)\, \mathbf{a}\,(\varphi_1)\right], \quad (26)$$

where $\mathcal{O}(\cdot)$ is the order operator, $\phi_1, \ldots, \phi_N$ are the *central* angles of the N bins, and φ_1 is a *random* angle in bin 1.

$$\mathbb{E}\left[\text{SINR}_\ell\right] \approx \frac{\rho_\text{t}\,\alpha_\ell\Big[p_2 + 2\left(L+1\right)p_1\,\sigma_\text{E}^2 + L\left(L+1\right)\sigma_\text{E}^2\Big]}{\frac{\sigma^2\left(p_1+L\sigma_\text{E}^2\right)}{N} + \rho_\text{t}\sum_{\substack{i=1\\ i\neq\ell}}^{L}\alpha_i\Big[p_4 + \sigma_\text{E}^2\,p_1 + L\,\sigma_\text{E}^4 + L\,\sigma_\text{E}^2\left(p_5+p_5^*\right) + \sigma_\text{E}^2\,p_1 + \ L\sigma_\text{E}^4\,p_3\Big]}. \tag{23}$$

$$\mathbb{E}\left[\text{SINR}_\ell\right] \approx \frac{\rho_\text{t}\,\alpha_\ell\Big[m_2 + 2\left(L+1\right)m_1\sigma_\text{E}^2 + L\left(L+1\right)\sigma_\text{E}^2\Big]}{\frac{\sigma^2\left(m_1+L\sigma_\text{E}^2\right)}{N} + \rho_\text{t}\sum_{\substack{i=1\\ i\neq\ell}}^{L}\alpha_i\Big[m_4 + 2\sigma_\text{E}^2 m_1 + \sigma_\text{E}^2 L\left(m_5+m_5^*\right)\Big]}. \tag{24}$$

Note that (26) follows by symmetry arguments as the terminal DOAs are $\mathcal{U}\left[0,2\pi\right]$. The expectations in (26) can be computed by application of the following mathematical result. Letting $q = \mathbb{E}\left[\mathbf{a}^H(\varphi)\,\mathbf{a}(\phi)\,\mathbf{a}^H(\phi)\,\mathbf{a}\left(\varphi\right)\right]$, one can write

$$q = \frac{1}{N^2}\sum_{s=1}^{N}\sum_{t=1}^{N} e^{jk_0(s-t)\Delta\sin(\phi)}\mathbb{E}\left[e^{jk_0(t-s)\Delta\sin(\varphi)}\right]. \tag{27}$$

If $\varphi \sim \mathcal{U}\left[a,b\right]$, the expectation in (27) can be written as

$$\mathbb{E}\left[e^{jk_0(t-s)\Delta\sin(\varphi)}\right] = \frac{1}{b-a}\int_a^b e^{jk_0(t-s)\Delta\sin(\varphi)}\,d\varphi, \tag{28}$$

where the integral can be efficiently evaluated using known results on incomplete Bessel functions or via simple closed–form approximations not shown here for reasons of space. For ease of notation, we denote the above integral as $J\left(a,b,jk_0\left(t-s\right)\Delta\right)$, which allows us to write (27) as

$$q = \frac{1}{N^2}\sum_{s=1}^{N}\sum_{t=1}^{N} e^{jk_0(s-t)\Delta\sin(\phi)}J\left(a,b,jk_0\left(t-s\right)\Delta\right). \tag{29}$$

The result in (29) is now extended, since it is required for the evaluation of other terms. We denote $\mu_{x,y,k} = \mathbb{E}\left[\mathbf{a}^H(\varphi_k)\,\mathbf{a}\left(\phi_x\right)\mathbf{a}^H(\phi_y)\,\mathbf{a}\left(\varphi_k\right)\right]$, such that

$$\mu_{x,y,k} = \frac{1}{N^2}\sum_{s=1}^{N}\sum_{t=1}^{N} e^{jk_0\Delta((s-1)\sin(\phi_x)-(t-1)\sin(\phi_y))} \times J\left(a_k,b_k,jk_0\left(t-s\right)\Delta\right), \tag{30}$$

and $[a_k,b_k]$ is the angular range of the k–th bin. This allows us to state

$$m_1 = \varsigma^2\mu_{1,1,1} + \frac{(L-1)}{(N-1)}\varsigma^2\sum_{s=2}^{N}\mu_{s,s,1}. \tag{31}$$

For reasons of space, in what follows, we quote the remaining results for m_2, m_4, and m_5. Starting with m_2, we have

$$m_2 = \varsigma^4\left[\hat{\mu}_{1,1} + \frac{2\left(L-1\right)}{(N-1)}\sum_{r=2}^{N}\hat{\mu}_{1,r} + \left(\frac{L-1}{N-1}\right)^2\sum_{r=2}^{N}\sum_{s=2}^{N}\hat{\mu}_{r,s}\right], \tag{32}$$

where $\hat{\mu}_{r,s}$ is defined in (33) on top of the following page. Similarly, m_4 is expressed as in (34) on top of the following page, where $\Re\left\{\cdot\right\}$ denotes the real component of a complex number. Finally, we can write m_5 as

$$m_5 = \frac{\varsigma^2}{N-1}\sum_{k=2}^{N}\left(\tilde{\mu}_{1,1,k} + \tilde{\mu}_{k,1,k} + \sum_{\substack{r=2\\ r\neq k}}^{L}\tilde{\mu}_{r,1,k}\right), \tag{35}$$

where $\tilde{\mu}_{x,k,r}$ is as defined in (36) on top of the following page.

Remark 5. *To the best of the authors' knowledge, these are the first set of analytical result on lens–based massive MIMO systems with imperfections in the RF lens and switching structure. The result derived in* (24) *is extremely general and is insensitive to changes in N, L, and ρ_t. While the numerical accuracy of the approximation is demonstrated in the following section, we note that* (24) *could be directly used to assess the ergodic sum spectral efficiency over all L user terminals via*

$$\text{R}_\text{sum}^\text{approx} \approx \sum_{\ell=1}^{L}\log_2\left(1+\mathbb{E}\left[\text{SINR}_\ell\right]\right). \tag{37}$$

The tightness of (37) *against its simulated counterpart is also numerically evaluated in the subsequent section.*

IV. Numerical Results

We assume that the carrier frequency $f_c = 28$ GHz and a coverage radius $R_\text{c} = 70$ m with LOS attenuation exponent $\eta = 2$. Each terminal is assumed to operate with the same uplink transmit power, while the noise power at the BS array, $\sigma^2 = 1$. This implies that ρ_t is the average operating SNR. We note that $\varphi_\ell \sim \mathcal{U}\left[0,2\pi\right]$, $\forall\ell = 1,2,\ldots,L$ and L terminals fall into L distinct bins. The inter–element spacing at the ULA interfacing the Rotman lens is $\Delta = 0.5\lambda$, while $\phi_\ell = \left(\ell-1\right)2\pi/N$, $\forall\ell = 1,2,\ldots,N$. Each of the following results are generated with 10^4 Monte–Carlo simulation realizations.

Figure 1 demonstrates the ergodic sum spectral efficiency of the system as a function of the average operating SNR with $N = 64$ and $L = 8$. Performance with an ideal lens and perfect RF switching is considered for comparison purposes as a useful upper limit. One can observe four trends from the figure: Firstly, imperfections in the RF switching matrix cause a more profound impact on the spectral efficiency relative to the case when perfect RF switching is assumed with imperfections in the Rotman lens (comparing the dashed line with the dotted one). While the spillover loss in the lens reduces the desired signal power as the lens is unable to focus the energy from a specific DOA to a specific beam port, it simultaneously helps in reducing the interference power, since the spreading of RF energy decorrelates the interference from multiple closely spaced directions. Secondly, the aggregate impact of both the imperfections leads to a significant loss of spectral efficiency at moderate and high ρ_t values. Thirdly, increasing the error variances of both imperfections by a small amount leads to a considerable degradation in the spectral efficiency particularly at high ρ_t values (comparing the dashed–dotted line with the last solid black line). This

$$\hat{\mu}_{r,s} = \frac{1}{N^4} \sum_{t=1}^{N} \sum_{u=1}^{N} \sum_{v=1}^{N} \sum_{w=1}^{N} e^{jk_0\Delta((t-u)\sin(\phi_r)+(v-w)\sin(\phi_s))} J\left(a_1, b_1, jk_0\left(u-t+w-v\right)\Delta\right). \tag{33}$$

$$m_4 = \frac{\varsigma^4}{N-1} \sum_{k=2}^{N} \mu_{1,1,k}\mu_{1,1,1} + \mu_{k,k,k}\mu_{k,k,1} + \sum_{\substack{r=1 \\ r\neq k}}^{N} \sum_{\substack{s=1 \\ s\neq k}}^{N} \mu_{r,s,k}\mu_{s,r,1} + 2\Re\left\{ \mu_{1,k,k}\,\mu_{k,1,1} + \sum_{\substack{r=1 \\ r\neq k}}^{N} \mu_{1,r,k}\mu_{r,1,1} + \sum_{\substack{r=1 \\ r\neq k}}^{N} \mu_{k,r,k}\mu_{r,k,1} \right\}. \tag{34}$$

$$\tilde{\mu}_{x,k,r} = \frac{1}{N^3} \sum_{s=1}^{N} \sum_{t=1}^{N} \sum_{u=1}^{N} e^{jk_0\Delta(u-s)\sin(\phi_x)} J\left(a_k, b_k, jk_0\left(s-t\right)\Delta\right) J\left(a_r, b_r, jk_0\left(t-u\right)\Delta\right). \tag{36}$$

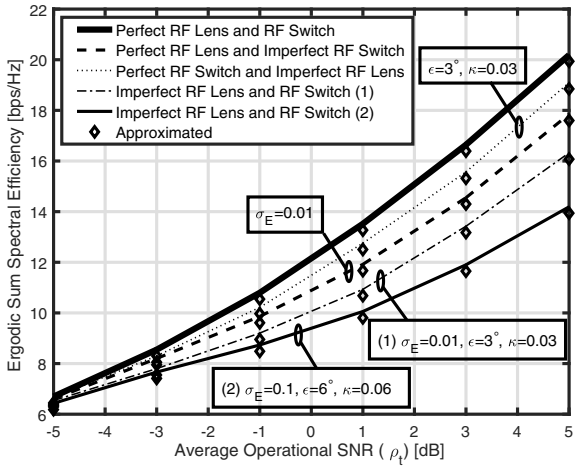

Fig. 1. Ergodic sum spectral efficiency vs. ρ_{t} with $N = 64$ and $L = 8$.

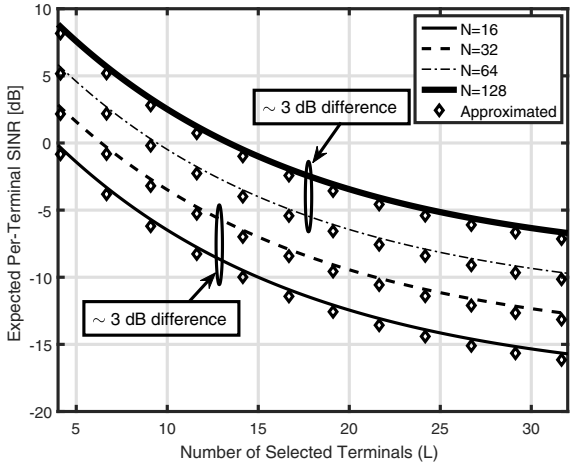

Fig. 2. Expected per–terminal SINR vs. L for different N, when $\rho_{\mathrm{t}} = 0$ dB.

demonstrates the sensitivity of the lens–based solutions to hardware impairments. Finally, the derived approximations are seen to closely predict the simulated responses for all considered cases. Overall, this result more accurately predicts the system performance with the considered imperfections, relative to the case when perfect system operation is assumed (routine assumption in the literature). To further demonstrate the accuracy of the derived approximations, Fig. 2 depicts the expected SINR as a function of increasing number of terminals with $\rho_{\mathrm{t}} = 0$ dB. Imperfections in both the lens and switching matrix are assumed with $\sigma_{\mathrm{E}} = 0.1$, $\epsilon = 6^{\circ}$ and $\kappa = 0.06$. One can observe that for a given N, the expected SINR decreases exponentially with increasing number of terminals. This is due to the higher probability of two terminals having a closely spaced DOA, leading to higher interference levels. One can notice that doubling the number of BS antennas yields an approximate 3 dB increase in the expected SINR for any considered number of user terminals.

V. Conclusions

Unlike previous studies, this paper models and analyzes the aggregate impact of imperfections in the Rotman lens (spillover losses) as well as the RF switching matrix (impedance mismatches and poor port isolation) in the context of a massive MIMO system. Assuming LOS propagation, tight analytical approximations of the expected SINR and ergodic sum spectral efficiency were derived with uplink MRC. Our results demonstrate significant degradation in expected SINR and spectral efficiency with the abovementioned imperfections, and provide a cautionary tale into performance sensitivity of lens–based architectures with these physical impairments.

References

[1] M. Shafi, *et al.*, "5G: A tutorial overview of standards, trials, challenges, deployment, and practice," *IEEE J. Sel. Areas Commun.*, vol. 35, no. 6, pp. 1201-1221, Jun. 2017.

[2] A. M. Sayeed and J. Brady, "Beamspace MIMO channel modeling and measurement: Methodology and results at 28GHz," in *Proc. IEEE GLOBECOM (Workshops)*, Dec. 2016.

[3] S. Park, *et al.*, "Dynamic subarrays for hybrid precoding in wideband mmWave MIMO systems," *IEEE Trans. Wireless Commun.*, vol. 16, no. 5, pp. 2907-2920, May 2017.

[4] V. Raghavan, *et al.*, "Single-user vs. multi-user precoding for millimeter-wave MIMO systems," *IEEE J. Sel. Areas Commun.*, vol. 35, no. 6, pp. 1387-1401, Jun. 2017.

[5] Z. Li, *et al.*, "Optimizing channel-statistics-based analog beamforming for millimeter-wave multiuser massive MIMO downlink," *IEEE Trans. Wireless Commun.*, vol. 16, no. 7, pp. 4288-4303, Jul. 2017.

[6] T. Kwon, *et al.*, "RF lens-embedded massive MIMO systems: Fabrication issues and codebook design," *IEEE Trans. Microw. Theory Tech.*, vol. 64, no. 7, pp. 2256-2271, Jul. 2016.

[7] Y. Gao, *et al.*, "Rotman lens based hybrid analog-digital beamforming in massive MIMO systems: Array architectures, beam selection algorithms and experiments", *IEEE Trans. Veh. Technol.*, vol. 66, no. 10, pp. 9134-9148, Oct. 2017.

[8] Y. Zeng and R. Zhang, "Millimeter wave MIMO with lens antenna array: A new path division multiplexing paradigm," *IEEE Trans. Commun.*, vol. 64, no. 4, pp. 1557-1571, Apr. 2016. .

[9] H. Tataria, *et al.*, "Uplink interference analysis with RF switching for lens-based millimeter-wave systems," in *Proc. IEEE ICC*, May 2018.

[10] Peregrine Semiconductors. Portfolio of RF Switches, accessed on Feb. 11, 2018. [Online]. Available: http://www.psemi.com/products/rf-switches.

[11] H. Tataria, *et al.*, "On the general analysis of coordinated regularized zero-forcing precoding: An application to two-tier small-cell networks," *IEEE Trans. Commun.*, vol. 65, no. 7, pp. 3133-3149, Jul. 2017.